Bioorganic & Medicinal Chemistry Letters 23 (2013) 4501–4505

Contents lists available at SciVerse ScienceDirect

Bioorganic & Medicinal Chemistry Letters

journal homepage: www.elsevier.com/locate/bmcl

Discovery of novel benzo[*b*][1,4]oxazin-3(4*H*)-ones as poly(ADP-ribose)polymerase inhibitors

Anthony R. Gangloff[a,*], Jason Brown[a], Ron de Jong[a], Douglas R. Dougan[a], Charles E. Grimshaw[a], Mark Hixon[a], Andy Jennings[a], Ruhi Kamran[a], Andre Kiryanov[a], Shawn O'Connell[b], Ewan Taylor[a] Phong Vu[a]

[a] *Takeda California, 10410 Science Center Dr, San Diego, CA 92121, USA*
[b] *Quanticel Pharmaceuticals, 9393 Towne Center Dr #110, San Diego, CA 92121, USA*

ARTICLE INFO

Article history:
Received 18 April 2013
Revised 13 June 2013
Accepted 17 June 2013
Available online 24 June 2013

Keywords:
Poly(ADP-ribose)polymerase inhibitors
PARP-1
Structure-based drug design
1,4-Benzoxazin-3-one
Chemopotentiation

ABSTRACT

Structure based drug design of a series of novel 1,4-benzoxazin-3-one derived PARP-1 inhibitors are described. The synthesis, enzymatic & cellular activities and pharmacodynamic effects are described. Optimized analogs demonstrated inhibition of poly-ADP-ribosylation in SW620 tumor bearing nude mice through 24 h following a single dose.

The enzyme poly(ADP-ribose)polymerase (PARP), previously known as poly(ADP-ribose)synthase and poly(ADP-ribosyl)transferase, constitutes a super family of proteins containing PARP catalytic domains involved in the repair of DNA, the regulation of cellular energy pools, and the transcription of inflammatory genes.[1] PARP-1 is a nuclear enzyme which catalyzes DNA repair through cleavage of NAD+ to nicotinamide and ADP-ribose to form long, branched ADP-ribose polymers on target proteins.[2] PARP-1 inhibition leads to sustained DNA damage and ultimately apoptosis when used in combination with DNA damaging agents such as temozolomide (TMZ), thus providing for chemopotentiation in vitro and in vivo.[3] PARP-1 inhibitors have also been shown to act as single agents through a form of synthetic lethality[4] by exploiting a DNA repair flaw seen in tumors expressing defective BRCA1/2-genes.[5] Therefore, inhibition of PARP-1 (which is over-expressed in tumors) is expected to hinder intracellular DNA repair and enhance the antitumor effects of cancer therapies.[6]

A key feature of PARP inhibitors is the ability to mimic nicotinamide binding to the backbone carbonyl and amide N–H of Gly202 as well as the O–H of Ser243 in the NAD pocket of PARP-1 (Fig. 1).[7] Hence, inhibitors containing a *cis*-amide capable of competing with NAD+ were considered to be a good starting point. A screening campaign identified several small fragments as weak PARP inhibitors, from which the 1,4-benz-oxazin-3-one core emerged as a promising chemotype. Using a published PARP-1 X-ray crystal structure,[8] benzoxazinone **2a** was overlaid onto the bound ligand present in the crystal structure (Fig. 2). Our analysis based on alignment of the *cis*-amide indicated the 6-position of the benzoxazinone to be a suitable initial starting point for extension into the back pocket to pick up interactions with the protein, although the 7-position could offer an additional vector. In addition, we anticipated that interactions with the hydrophobic shelf could be achieved through substitution on the 2- and 8-position of the benzoxazinone core.

The initial compounds were synthesized as outlined in Scheme 1. Alkylation of substituted *o*-nitrophenols was accomplished in >70% yield using α-bromoacetates in DMF with K_2CO_3. Reduction of the nitro group and subsequent cyclization of the resultant amine was achieved in a single step using iron dust in AcOH at 80 °C. Reductive amination when R^3 is a formyl group introduced substituents which could extend into the back pocket.

A notable observation was that a methyl group at the 2-position increased both binding potency against PARP-1 and ligand-lipophilic efficiency[10] (LLE) as demonstrated by the benzoxazinone fragments **2a** and **2d** where the 2-methyl group confers an order of magnitude improvement in inhibitory activity (Table 1). In the case of **3d** and **3e**, the K_d was increased by two log units and LLE by 1.5 log units. These observations can be explained by the presence of a proximal narrow hydrophobic cleft (defined by

* Corresponding author. Tel.: +1 858 731 3531; fax: +1 858 550 0526.
E-mail address: anthony.gangloff@takeda.com (A.R. Gangloff).

0960-894X/$ - see front matter © 2013 Elsevier Ltd. All rights reserved.
http://dx.doi.org/10.1016/j.bmcl.2013.06.055

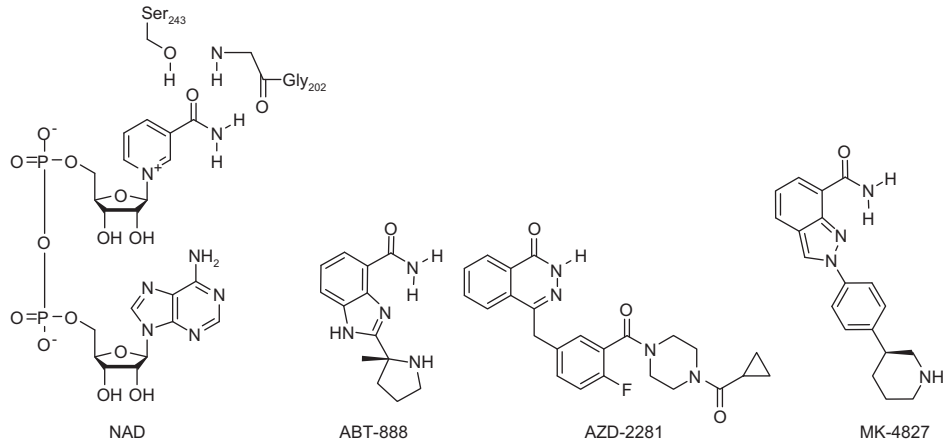

Figure 1. Structures of reported PARP inhibitors and NAD+ with PARP-1 catalytic domain.

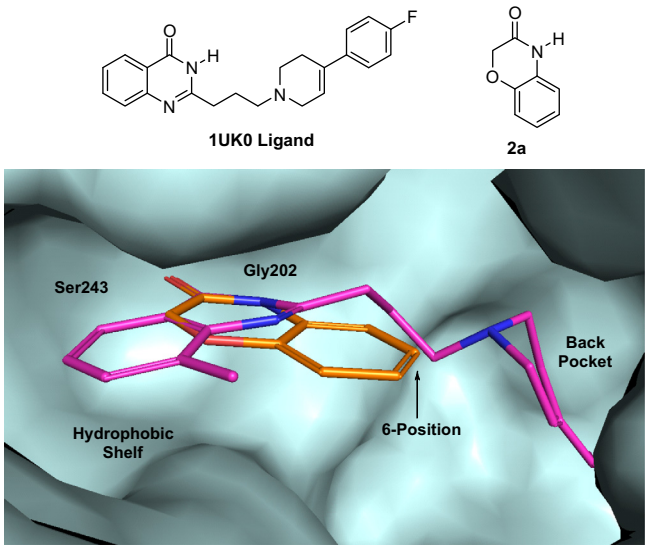

Figure 2. Overlay of 1UK0 ligand in PARP-1 with benzoxazinone **2a**.

Phe897 and Tyr896) which exists in the active site, and the 2-methyl group is optimally sized and positioned to for Van der Waal's interactions with these residues. Bis-substitution on C-2 such as **2g** resulted in 15-fold reduced binding potency. Occupation of the back pocket as in **3e**, **3g** and **3j** resulted in sub-micromolar activity and further increases in LLE. Optimizing substituents for accessing the back pocket from the benzoxazinone 6-position with the tetrahydropyridine moiety in **3j** produces sub-10 nM potency against PARP-1. The X-ray crystal structure of **3j** clearly shows both the hydrophobic shelf occupied by the C-2 methyl and also the trajectory of the chlorophenyl group off the tetrahydropyridine ring into the back pocket (Fig. 3). The importance of the regiochemistry for the vector off the benzoxazinone is clearly demonstrated when comparing 6-substituted **3g** (0.046 μM) and 7-substituted **3h** (10 μM), and likewise with regioisomeric **3j** (0.003 μM) and **3k** (100 μM). Larger substituents at R^1 lead to a greater than 30,000-fold loss of binding potency such as the ethyl group in **3l** (100 μM) compared to its methyl analog **3j** (0.003 μM). Overall, efficiency was improved compared to the fragment starting point **2d** with LLE values ranging from 4.5 to 4.9.

Although sub-100 nM PARP-1 inhibitors had been identified, cellular potentiation was lacking for all compounds in Table 1. There are many possible reasons for the lack of cellular activity, including the inability of the inhibitors to engage intranuclear PARP since the nuclear membrane is less permeable to xenobiotics than the cellular membrane.[11] One strategy for improving cellular potency was to design compounds with reduced Log*D* and lipohilicity (*c*Log*D* values for **3g**–**3i** fell within the range of 3.3–3.9) could be attenuated. One approach to reduce log*D* values was to replace the piperidine or tetrahydropyridine moiety present in compounds **3f**–**3l** with a piperazine group and optimizing the phenyl substituents, thus lowering the Log*D* to an lower value of <3.0. Exploration of back pocket interactions seen in Fig. 3 was enabled through appropriate substitutions on the phenyl ring with potential for hydrogen bonding with Ile879 and/or Arg878. The X-ray co-crystal structure[12] of **3j** also showed there was room for substitution at the 8-position of the benzoxazinone core to allow for

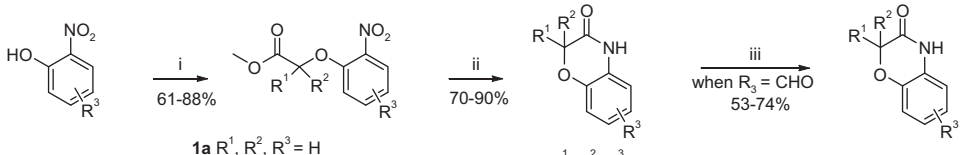

1a R^1, R^2, R^3 = H
1b R^1, R^2 = H, R^3 = 6-CHO
1c R^1, R^2 = H, R^3 = 6-C(O)Me
1d R^1 = Me, R^2, R^3 = H
1e R^1 = Me, R^2 = H, R^3 = 6-CHO
1f R^1, R^2 = Me, R^3 = H
1g R^1 = Me, R^2 = H, R^3 = 7-CHO
1h R^1 = Et, R^2 = H, R^3 = 6-CHO

2a R^1, R^2, R^3 = H
2b R^1, R^2 = H, R^3 = 6-CHO
2c R^1, R^2 = H, R^3 = 6-C(O)Me
2d R^1 = Me, R^2, R^3 = H
2e R^1 = Me, R^2 = H, R^3 = 6-CHO
2f R^1, R^2 = H, R^3 = Et
2g R^1, R^2 = Me, R^3 = H
2h R^1 = Me, R^2 = H, R^3 = 7-CHO
2i R^1 = Et, R^2 = H, R^3 = 6-CHO

3

Scheme 1. Reagents and conditions: (i) $BrCR^1R^2CO_2Me$, K_2CO_3, DMF, 80 °C; (ii) iron dust, AcOH, 80 °C; (iii) R^3NH_2, $NaBH(OAc)_3$, AcOH, DCE, 23 °C; (iv) Et_3SiH, TFA, 80 °C.

Table 1
PARP-1 binding potencies and efficiency metrics for benzoxazinones **2**–**3**

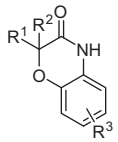

Compound [a]	R^1	R^2	R^3	PARP-1[b] K_d (μM)	PARP-1[c] LLE
2a	H	H	H	>500	
2d	Me	H	H	32	2.3
2g	Me	Me	H	>500	
2b	H	H	6-Formyl	170	2.0
2f	H	H	6-Ethyl	100	2.0
3a	H	H	6-PhenylNHCH$_2$	26	2.2
3b	H	H	6-BenzylNHCH$_2$	11	3.5
3c	Me	H	6-BenzylNHCH$_2$	5.2	3.2
3d	H	H	6-(4-(Me$_2$N)piperidine)CH$_2$	15	3.0
3e	Me	H	6-(4-(Me$_2$N)piperidine)CH$_2$	0.096	4.6
3f	H	H	6-(4-(Phenyl)piperidine)CH$_2$	0.296	3.4
3g	Me	H	6-(4-(Phenyl)piperidine)CH$_2$	0.046	3.7
3h	Me	H	7-(4-(Phenyl)piperidine)CH$_2$	10	1.4
3i	H	H	6-(4-(4-Chlorophenyl)-1,2,3,6-tetrahydropyridine)CH$_2$	0.015	4.5
3j	Me	H	6-(4-(4-Chlorophenyl)-1,2,3,6-tetrahydropyridine)CH$_2$	0.003	4.9
3k	Me	H	7-(4-(4-Chlorophenyl)-1,2,3,6-tetrahydropyridine)CH$_2$	100	0.2
3l	Et	H	6-(4-(4-Chlorophenyl)-1,2,3,6-tetrahydropyridine)CH$_2$	100	0.1

[a] When applicable, compounds are racemic.
[b] Determined using SPR[9], $n = 2$.
[c] LLE = pK_d − cLog$D$.

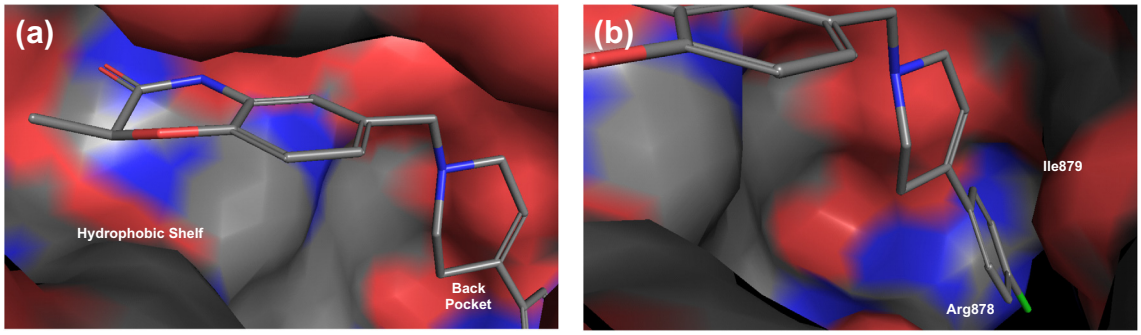

Figure 3. X-ray crystal structure of **3j** (S-enantiomer shown) (a) binding pocket view (b) back pocket view.

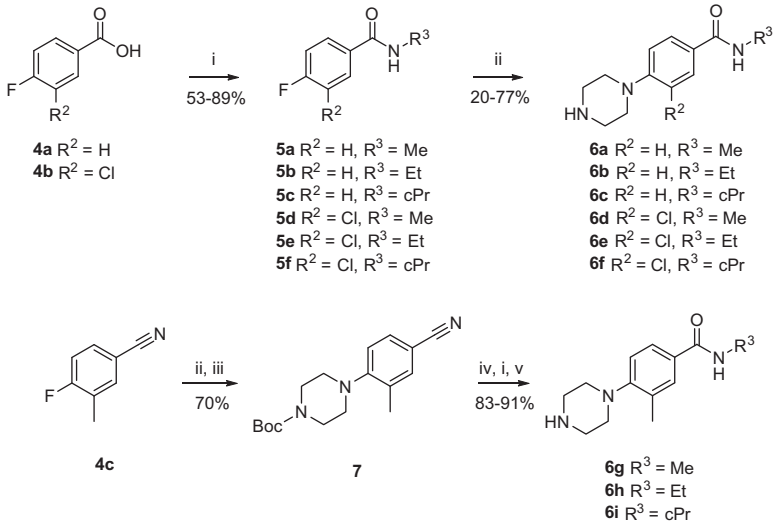

Scheme 2. Reagents and conditions: (i) R^3NH_2, EDC, HOBt, NMM, DMF, 23 °C; (ii) piperazine, DMSO, 120 °C; (iii) Boc_2O, THF, MeOH, 23 °C; (iv) NaOH, EtOH, H_2O, 90 °C; (v) HCl, dioxane, 23 °C.

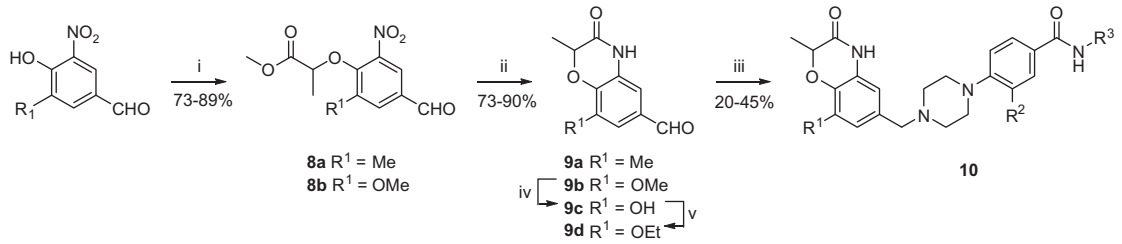

Scheme 3. Reagents and conditions: (i) $BrCHMeCO_2Me$, K_2CO_3, DMF, 80 °C; (ii) iron dust, AcOH, 80 °C; (iii) **6**, $NaBH(OAc)_3$, AcOH, DCE, 23 °C; (iv) BBr_3, DCM, −10 °C; (v) Et-I, $CsCO_3$, DMF, 0 °C.

Table 2
Enzymatic and cellular activity for benzoxazinones **10**

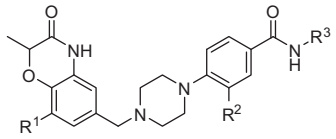

Compound[a]	R^1	R^2	R^3	PARP-1[b] IC_{50} (nM)	Cell EC_{50}[c] w/TMZ (μM)	Cell EC_{50} w/o TMZ (μM)	Cell PF_{50}
10a	H	H	Me	29	15	14	1.0
10b	H	H	Et	22	15	42	2.8
10c	H	Cl	Et	18	4	100	20
10d	Me	H	Me	17	11	75	6.8
10e	Me	H	Et	6	9	94	10.4
10f	Me	H	cPr	33	5	100	20
10g	OMe	H	Me	29	27	251	9.3
10h	OMe	H	Et	23	16	151	9.4
10i	OMe	H	cPr	30	16	162	10.1
10j	Me	Cl	Me	49	14	45	3.2
10k	Me	Cl	Et	89	14	47	3.4
10l	Me	Cl	cPr	76	0.01	43	4300
10m	Me	Me	Me	38	9	78	8.7
10n	Me	Me	Et	56	9	55	6.1
10o	Me	Me	cPr	52	18	100	5.6
10p	OMe	Me	Me	36	0.06	100	1667
10q	OMe	Me	Et	32	0.01	44	4400
10r	OMe	Me	cPr	147	0.02	77	3850
10s	OEt	Me	Me	35	0.02	26	1300
10t	OEt	Me	Et	55	0.02	100	5000
10u	OEt	Me	cPr	41	0.02	100	5000
ABT-888	—	—	—	16	3	160	56
AZD-2281	—	—	—	6	0.06	16	660
MK-4827	—	—	—	35	0.20	31	160

[a] Compounds are racemic.
[b] Determined using Trevigen assay, $n = 2$, av SD = 8 nM.
[c] TMZ = 100 μM.

interaction with the hydrophobic shelf and further optimization of physicochemical properties.

The desired piperazines **6a–i** were prepared using coupling and nucleophilic aromatic substitution reactions (Scheme 2). Scheme 3 outlines the preparation of compounds **10** exemplified in Table 2 in which all three substituent possibilities are exemplified: substitution at the benzoxazinone core (8-position R^1), and back-pocket phenyl group substitution (R^2 and R^3).

Cellular potency was determined in duplicate in the Jurkat cell line using a cell viability assay that measured the conversion of MTS after 96 h treatment with serially diluted compound in the presence or absence of TMZ. Chemopotentiation factor (PF_{50}) was calculated as the ratio of EC_{50} values of cells co-treated with and without TMZ, respectively.[13]

Biological evaluation showed R^2 substitution maintained enzymatic potency (**10b–c**,Table 2).[14] However, **10c** where R^2 is chloro shows the first hint of chemopotentiation (PF_{50} = 20). When R^2 = H (**10d–i**), cellular chemopotentiation showed no improvement over **10c** and the optimal substituent for R^2 is methyl. The first

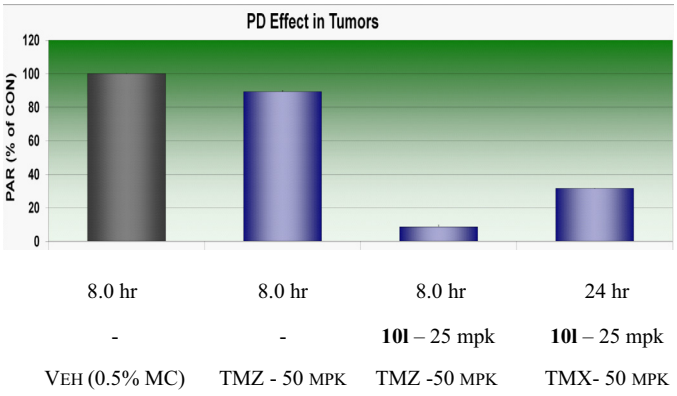

Figure 4. Pharmacodynamic effects of **10l** in SW-620 tumor xenografts.[15]

compound with >100-fold cellular chemopotentiation was **10l** where all three positions are substituted. Compounds **10p** through **10u** have an alkoxy substitutent at R^1 and methyl at R^2. Chemopotentiation was improved when R^3 is ethyl or cyclopropyl compared to methyl. Such optimal substitution patterns resulted in chemopotentiation factors above 1000. When compared to the clinical compounds in Figure 1, the benzoxazinones showed chemopotentiation factors with an order of magnitude improvement in many cases despite being 3- to 6-fold less potent in the enzymatic assay. Our objective to design higher quality compounds ($c\mathrm{Log}D$ <3.0) which maintained the enzymatic potencies seen in Table 1 but also displayed chemopotentiation in cellular systems had been demonstrated.

The increased chemopotentiation seen with **10l** resulted in a pharmacodynamic effect in tumor bearing mice, preventing poly-ADP-ribosylation in SW-620 tumor xenografts at 8 and 24 h post dose (Fig. 4).[15] SW-620 (a p53−/− human colorectal adenocarcinoma cell line) was implanted into nude mice and allowed to grow to ~325 ±75 mg. The PARP inhibitor **10l** was dosed orally with TMZ (50mpk). Tumors were removed 8 or 24 h after dosing, homogenized, normalized for total protein and the lysates were analyzed using Trevigen ELISA (Cat. #: 4510-096-K). A strong and sustained tumor pharmacodynamic response was observed with **10l** maintaining inhibition of poly-ADP-ribosylation through 24 h.

The major liability of the PARP inhibitors described above which prevented further development was hERG inhibition. Compounds **10p**, **10q**, and **10s** all exhibited >97% inhibition of the hERG channel in an electrophysiology assay at 10 μM.

In summary, PARP inhibitors have been developed from a fragment screening campaign utilizing structure-based drug design principles to yield novel benzoxazinones displaying sub-100 nM potency in enzymatic assays and cellular potentiation factors greater than 1000. When optimally substituted, the compounds show an improvement in synergy over PARP inhibitors currently in clinical development. The increased cellular activity translated to an in vivo pharmacodynamic response with sustained inhibition for 24 h. Further development of the benzoxazinone scaffold into drug-like inhibitors which demonstrate in vivo efficacy and overcome a hERG liability seen in the above compounds has been pursued. The inhibitors described here provide additional tools to explore the role of PARP-1 in cancer and other diseases.

Acknowledgments

We thank Dr. Matthew Marx and Dr. Gavin Hirst for their critical reading of the manuscript, Dr. Clifford D. Mol for crystallography work and Philip Erickson for chemical synthesis.

Supplementary data

Supplementary data associated with this article can be found, in the online version, at http://dx.doi.org/10.1016/j.bmcl.2013.06.055.

References and notes

1. Rouleau, M.; Patel, A.; Hendzel, M. J.; Kaufmann, S. H.; Poirier, G. G. *Nat. Rev. Cancer* **2010**, *10*, 293.
2. Chambon, P.; Weil, J. D.; Mandel, P. *Biochem. Biophys. Res. Commun.* **1963**, *11*, 39.
3. Delaney, C. A.; Wang, L. Z.; Kyle, S.; White, A. W.; Calvert, A. H.; Curtin, N. J.; Durkacz, B. W.; Hostomsky, Z.; Newell, D. R. *Clin. Cancer Res.* **2000**, *6*, 2860; Miknyoczki, S. J.; Jones-Bolin, S.; Pritchard, S.; Hunter, K.; Zhao, H.; Wan, W.; Ator, M.; Bihovsky, R.; Hudkins, R.; Chatterjee, S.; Klein-Szanto, A.; Dionne, C.; Ruggeri, B. *Mol. Cancer Ther.* **2003**, *2*, 371; Calabrese, C. R.; Batey, M. A.; Thomas, H. D.; Durkacz, B. W.; Wang, L. Z.; Kyle, S.; Skalitzky, D.; Li, J.; Zhang, C.; Boritzki, T.; Maegley, K.; Calvert, A. H.; Hostomsky, Z.; Newell, D. R.; Curtin, N. J. *Clin. Cancer Res.* **2003**, *9*, 2711; Donawho, C. K.; Luo, Y.; Penning, T. D.; Bauch, J. L.; Bouska, J. J.; Bontcheva-Diaz, V. D.; Cox, B. F.; DeWeese, T. L.; Dillehay, L. E.; Ferguson, D. C.; Ghoreishi-Haack, N. S.; Grimm, D. R.; Guan, R.; Han, E. K.; Holley-Shanks, R. R.; Hristov, B.; Idler, K. B.; Jarvis, K.; Johnson, E. F.; Kleinberg, L. R.; Klinghofer, V.; Lasko, L. M.; Liu, X.; Marsh, K. C.; McGoniga, T. P.; Meulbroek, J. A.; Olson, A. M.; Palma, J. P.; Rodriguez, L. E.; Shi, Y.; Stavropoulos, J. A.; Tsurutani, A. C.; Zhu, G. D.; Rosenberg, S. H.; Giranda, V. L.; Frost, D. J. *Clin. Cancer Res.* **2007**, *13*, 2728.
4. Leung, M.; Rosen, D.; Fields, S.; Cesano, A.; Budman, D. R. *Mol. Med.* **2011**, *17*, 854.
5. Bryant, H. E.; Schultz, N.; Thomas, H. D.; Parker, K. M.; Flower, D.; Lopez, E.; Kyle, S.; Meuth, M.; Curtin, N. J.; Helleday, T. *Nature* **2005**, *434*, 913; Farmer, H.; McCabe, N.; Lord, C. J.; Tutt, A. N.; Johnson, D. A.; Richardson, T. B.; Santarosa, M.; Dillon, K. J.; Hickson, I.; Knights, C.; Martin, N. M.; Jackson, S. P.; Smith, G. C.; Ashworth, A. *Nature* **2005**, *434*, 917; Balmana, J.; Domchek, S. M.; Tutt, A.; Garber, J. E. *Cancer Disc.* **2011**, *1*, 29.
6. Ferraris, D. V. *J. Med. Chem.* **2010**, *53*, 4561.
7. Residues numbered as found in the PDB file 1UK0.
8. Kinoshita, T.; Nakanishi, I.; Warizaya, M.; Iwashita, A.; Kido, Y.; Hattori, K.; Fujii, T. *FEBS Lett.* **2004**, *556*, 43.
9. Complete details for SPR determination can be found in the Supplementary data.
10. Edwards, M. P.; Price, D. A. *Annu. Rep. Med. Chem.* **2010**, *45*, 380.
11. Chi, Y.-H.; Chen, Z.-J.; Jeang, K.-T. *J. Biomed. Sci.* **2009**, 16.
12. The coordinates of compound **3j** have been deposited in the RCSB Protein Data Bank (PDB ID code 4L6S). To obtain the co-crystal structure, racemic **3j** was utilized but only the S-enantiomer was seen in the resulting structure. Based on modeling, both enantiomers are possible but S- is preferred.
13. Jurkat cells were seeded in 96-well tissue culture microplates at 10,000 cells per well and cultured for 24 h prior to addition of compounds, TMZ (Temozolomide) or DMSO (dimethylsulfoxide) vehicle. After 96 h, conversion of MTS by metabolically active cells was determined. Cells were treated in duplicate with a range of serial compound dilutions in the absence or presence of 100 μM TMZ. Complete details can be found in the Supplementary data.
14. Inhibition of PARP catalytic activity was determined by use of an ELISA-based colorimetric PARP/Apoptosis Assay kit (part number 4684-096-K HT, Trevigen). Complete details can be found in the Supplementary data.
15. 3 animals per group. Vehicle for all groups was 0.5% methylcellulose. Average standard deviation was 0.14 (Vehicle), 0.36 (TMZ), 0.81 (**10l**, 8 h), 0.14 (**10l**, 24 h).